Author version: *Nature, vol.487; 2012; 313-319*

Deep carbon export from a Southern Ocean iron-fertilized diatom bloom

Victor Smetacek[1,2*], Christine Klaas[1*], Volker H. Strass[1], Philipp Assmy[1,3], Marina Montresor[4], Boris Cisewski[1,5], Nicolas Savoye[6,7], Adrian Webb[8], Francesco d'Ovidio[9], Jesús M. Arrieta[10,11], Ulrich Bathmann[1,12], Richard Bellerby[13,14], Gry Mine Berg[15], Peter Croot[16,17], Santiago Gonzalez[10], Joachim Henjes[1,18], Gerhard J. Herndl[10,19], Linn J. Hoffmann[16], Harry Leach[20], Martin Losch[1], Matthew M. Mills[15], Craig Neill[13,21], Ilka Peeken[1,22], Rüdiger Röttgers[23], Oliver Sachs[1,24], Eberhard Sauter[1], Maike M. Schmidt[25], Jill Schwarz[1,26], Anja Terbrüggen[1], & Dieter Wolf-Gladrow[1]

[1]Alfred Wegener Institute for Polar and Marine Research, Am Handelshafen 12, 27570 Bremerhaven, Germany.

[2]National Institute of Oceanography, Dona Paula, Goa 403 004, India.

[3]Norwegian Polar Institute, Hjalmar Johansens gt. 14, Fram Centre, 9296 Tromsø, Norway.

[4]Ecology and Evolution of Plankton, Stazione Zoologica 'A. Dohrn', Villa Comunale, 80121-Napoli, Italy.

[5]Johann Heinrich von Thünen-Institute, Institute of Sea Fisheries, Palmaille 9, 22767 Hamburg, Germany.

[6]Department of Analytical and Environmental Chemistry, Vrije Universiteit Brussel, Pleinlaan 2, 1050 Brussels, Belgium.

[7]Univ. Bordeaux / CNRS, EPOC, UMR 5805, Station Marine d'Arcachon, 2 rue du Professeur Jolyet, 33120 Arcachon, France.

[8]Oceanography Department, University of Cape Town, Private Bag X3, Rondebosch, 7701 Cape Town, South Africa.

[9]LOCEAN-IPSL, CNRS/UPMC/IRD/MNHN, 4 place Jussieu, 75252 Paris Cedex 5 (France).

[10]Department of Biological Oceanography, Royal Netherlands Institute for Sea Research (NIOZ), P.O. Box 59, 1790AB, The Netherlands.

[11]Department of Global Change Research, Instituto Mediterraneo de Estudios Avanzados (IMEDEA), CSIC-UIB, Miquel Marques 21, 07190 Esporles, Mallorca, Spain.

[12] Leibniz Institute for Baltic Sea Research Warnemünde, Seestraße 15, 18119 Rostock, Germany

[13]Bjerknes Centre for Climate Research, University of Bergen, Allegaten 55, N-5007 Bergen, Norway.

[14]Norwegian Institute for Water Research, Thormøhlensgate 53 D, 5006 Bergen, Norway.

[15]Department of Environmental Earth System Science, Stanford University, Stanford, CA 94305, USA.

[16]Helmholtz Centre for Ocean Research Kiel (GEOMAR), Düsternbrooker Weg 20, 24105 Kiel, Germany.

[17]Earth and Ocean Sciences, School of Natural Sciences, National University of Ireland, Galway (NUIG), Quadrangle Building, University Road, Galway, Ireland.

[18]Phytolutions GmbH, Campus Ring 1, 28759 Bremen, Germany.

[19]Department of Marine Biology, University of Vienna, Althanstrasse 14, 1090 Vienna, Austria.

[20]School of Environmental Sciences, University of Liverpool, Room 209 Nicholson Building, 4 Brownlow Street, Liverpool, L69 3GP, UK.

[21]Wealth from Oceans Flagship, Commonwealth Scientific and Industrial Research Organisation, Castray Esplanade, Hobart, TAS 7000, Australia.

[22]MARUM - Center for Marine Environmental Sciences, University of Bremen, Leobener Str., D-28359 Bremen, Germany.

[23]Institute for Coastal Research, Helmholtz-Zentrum Geesthacht, Center for Materials and Coastal Research, Max-Planck-Str. 1, 21502 Geesthacht, Germany.

[24]Eberhard & Partner AG, General Guisan-Strasse 2, 5000 Arau, Switzerland.

[25]Centre for Biomolecular Interactions Bremen, FB 2, University of Bremen, Postfach 33 04 40, 28359 Bremen, Germany.

[26]School of Marine Science & Engineering, Plymouth University, Drake Circus, Plymouth PL4 8AA, UK.

* These authors contributed equally to this work

Ocean iron fertilization experiments have induced diatom-dominated phytoplankton blooms accompanied by significant CO_2 drawdown in the surface layer. However, since the fate of bloom biomass could not be adequately resolved, the time scales of carbon sequestration from the atmosphere are uncertain. We carried out a five-week experiment in the closed core of a vertically coherent, mesoscale eddy of the Antarctic Circumpolar Current and tracked sinking particles from the surface to the deep-sea floor. A large diatom bloom peaked in the fourth week after fertilization followed by mass mortality of several diatom species that formed rapidly-sinking mucilaginous aggregates of entangled cells and chains. Taken together, multiple lines of evidence - albeit each with important uncertainties – lead us to conclude that at least half the bloom biomass sank well below 1,000 m depth and a substantial portion is likely to have reached the sea floor. Thus, iron-fertilized diatom blooms may sequester carbon in the deep ocean for time scales of centuries and longer.

The Southern Ocean is regarded as a likely source and sink of atmospheric CO_2 over glacial/inter-glacial climate cycles but the relative importance of physical and biological mechanisms driving CO_2 exchange are under debate[1,2]. The iron hypothesis[3], based on iron-limitation of phytoplankton growth in extensive, nutrient-rich areas of today's oceans, proposes that the greater supply of iron-bearing dust to these regions during the dry glacials stimulated phytoplankton blooms which, by sinking out to the deep ocean, sequestered relevant amounts of carbon from exchange with the atmosphere. A dozen ocean iron fertilization (OIF) experiments carried out to test this hypothesis have provided unambiguous support for the first condition: that iron addition generates phytoplankton blooms in regions with high nutrient but low chlorophyll concentrations (HNLC regions) including the Southern Ocean[4,5]. The findings are consistent with satellite observations of natural phytoplankton blooms in these regions stimulated by dust input from continental[6] and volcanic[7] sources.

The time scales at which CO_2 taken up by phytoplankton is sequestered from the atmosphere depends on the depths at which organic matter sinking out of the surface layer is subsequently remineralised back to CO_2 by microbes and zooplankton. In the Southern Ocean the portion of CO_2 retained within the 200 m deep winter-mixed layer would be in contact with the atmosphere within months but carbon sinking to successively deeper layers, and finally the sediments, will be sequestered for decades to centuries or longer. Previous OIF experiments have not adequately demonstrated the fate and depth of sinking of bloom biomass[5], so it is uncertain whether mass, deep-sinking events comparable to those observed in the aftermath of natural blooms[8] also ensue from OIF blooms. Further, palaeoceanographic proxies from the underlying sediments are ambiguous regarding productivity of the glacial Southern Ocean[1,2,9, 10]. Hence, the second condition of the iron hypothesis, that OIF generated biomass sinks to greater depths, has yet to be confirmed. The issue is currently receiving broad attention as OIF is one of the techniques listed in the geoengineering portfolio to mitigate the effects of climate change[11].

Monitoring the sinking flux from an experimental bloom requires vertical coherence between surface and deeper layers, a condition fulfilled by the closed cores of mesoscale eddies formed by meandering frontal jets of the Antarctic Circumpolar Current (ACC) that are prominent in satellite altimeter images as sea-surface height anomalies (SSHA)[12]. An added advantage is that processes occurring in the fertilized patch can be compared with natural processes in adjoining unfertilized waters of the same provenance.

The eddy and experiment

The European Iron Fertilization Experiment (EIFEX) was carried out from February 11 (Day -1) to March 20, 2004 (Day 36), in the clockwise-rotating core of an eddy, formed by a meander of the Antarctic Polar Front (APF) (Fig 1; Supplementary Information). The eddy was mapped shortly after fertilization of the patch (from Days 1–7) with a grid of 80 stations along 8 north/south transects 9 km apart, during which the rotating patch was encountered on two of the grid transects. Underway measurements of current speed and direction with the vessel-mounted ADCP system and SSHA images revealed a closed core of 60 km diameter clearly demarcated from the surrounding meander of the Polar Front by all measured physical, chemical and biological properties (Fig. 1a and 1b, Supplementary Information).

Estimates of geostrophic shear and transports derived from temperature and salinity profiles (Supplementary Fig. 1 and 2) indicate a coherent surface-to-bottom eddy circulation that was almost closed with little divergence. The vertical coherence of the eddy was also revealed by the congruent tracks of 4 neutrally buoyant floats parked at 200 m, 300 m, 500 m, and 1000 m depth (Supplementary Fig. 3). A post-cruise Lagrangian analysis based on delayed-time altimetry[13] showed that, for the entire duration of the experiment, the compact core was only marginally eroded by lateral stirring, losing less than 10% of its content over the 37 days of the experiment (Supplementary Information). This finding is consistent with diffusive heat budgets derived from the observed warming of the eddy's cold core[14]. Hence, the EIFEX eddy provided ideal conditions for monitoring the same water column from the surface to the sea floor over time.

The site of the pre-fertilization control station taken on Day -1 was marked with a drifting buoy around which a circular patch of 167 km^2 was fertilized with dissolved ferrous sulphate on Day 0 to yield a concentration of 1.5 µmol Fe m^{-3} in the 100 m surface mixed layer, around 5-fold above background values. A second fertilization on Days 13 and 14 added an additional 0.34 µmol Fe m^{-3} to the 100 m surface layer of the spreading patch. The patch was inadvertently placed off-centre but well within the closed eddy core and completed 4 rotations from Days 0-36. Patch area increased from 167 km^2 on Day 0 to 447 km^2 on Day 11 and 798 km^2 on Day 19 (Fig 1 c-f, Supplementary Information). "In-stations" were taken in the least-diluted region of the patch: the "hotspot" (Fig. 1 c-f). "Out-stations" were taken within the eddy core well away from the patch but in different locations relative to it, hence did not represent ideal controls for quantifying processes within the patch.

Sampling frequency and depth coverage by discrete measurements are illustrated by vertical distribution of chlorophyll and silicate concentrations in Fig 2. Vertical profiles of in-situ recording instruments indicated that the mixed layer depth, defined by the sharp dip in temperature, salinity, fluorescence and transmission profiles, was generally at 100 m depth[15] (97.6 ± 20.6 m). The element and biomass budgets presented here are based on inventories (mol or g m^{-2}) derived from trapezoidal integration of 6 – 8 discrete measurements from the surface 100 m layer. For comparison with other studies the 100 m stocks and inventories are also presented where appropriate as depth-averaged concentrations (mmol or mg m^{-3}).

Processes inside and outside the patch

Enhanced phytoplankton growth stimulated by iron fertilization resulted in highly significant, linear increases of stocks (inventories) of chlorophyll (Chl), particulate organic carbon (POC), nitrogen (PON), phosphate (POP) and biogenic silica (BSi) until day 24 (Fig. 2a and Fig. 3). These stocks, depicted as depth-averaged concentrations in Fig. 3, declined thereafter albeit at different rates. However, inventories of the corresponding dissolved nutrients, including dissolved organic nitrogen (DON), exhibited constant, linear decline until the end of the experiment indicating that the respective uptake rates were maintained throughout (Fig 3). Detailed, visual, quantitative examination of organisms and their remains across the entire size spectrum of the plankton revealed that population growth of many different species of large diatoms accounted for 97% of the Chl increase. The decline was caused by mass death and formation of rapidly sinking aggregates by some diatom species which was partly compensated by continued growth of other, heavily silicified species with high accumulation rates. The strikingly linear, instead of exponential, trends can be attributed to the effects of patch dilution with surrounding water because dilution rates (0.06 - 0.1 d^{-1}, Supplementary Information) and phytoplankton accumulation rates (0.03 – 0.11 d^{-1}) were similar.

The discrepancies in budgets of particulate and dissolved pools of the various elements in the surface layer can only be explained by sinking out of particles, as losses to dissolved organic pools can largely be ruled out: Dissolved organic carbon (DOC) stocks remained stable (44 ± 2 mmol C m^{-3}) (Fig. 3l), DON declined twofold (from 3.8 to 2.0 mmol N m^{-3}) (Fig. 3f) and dissolved organic phosphate (not shown) concentrations were at the detection limit. The DON decline was barely reflected in DOC because it was apparently associated with a relatively small, labile fraction with much lower C/N ratios than that of the large refractory DOC pool.

The post-fertilization eddy survey revealed that the patch was located in the region of the eddy core with the highest silicate and lowest chlorophyll concentrations (~0.7 mg Chl m^{-3}) (Supplementary

Information). Patchy, natural blooms, probably caused by local dust input along the APF[6], had occurred prior to our arrival adjacent to the patch (Fig. 1g), indicated by lower nutrient, higher Chl stocks (up to 1.2 mg Chl m^{-3}) and higher particle loads in subsurface layers (Supplementary Information). These natural blooms sank from the surface in the first week, corroborated by barite profiles in subsurface layers[16], hence higher particle stocks encountered at depth at some out stations in all likelihood stemmed from them. Particle stocks (except BSi) in the upper 100 m layer outside the patch continued declining by about 50% during the 5 weeks (Fig. 3) due to steady sinking out of particles as indicated by the discrepancy between temporal evolution of dissolved and particulate inventories of the respective elements. A brief visit to the eddy core on Day 50 found Chl concentrations had declined further to 0.1 mg Chl m^{-3}.

Export from the iron-induced bloom

Vertical particle flux (export) induced by iron fertilization was estimated for the hotspot from: a) losses of biogenic element inventories in the surface layer, including ^{234}Thorium, b) increase in POC in the underlying deep water column, c) balance between rates of primary production and heterotrophic activity. These estimates represent total export and include losses incurred by the surface layer in the absence of fertilization (background flux). Because some out-stations were affected by patchy natural blooms within the eddy core, they did not represent ideal controls. However, export rates from the fertilized patch, estimated from elemental budgets in the surface layer (0 - 100 m) and particularly POC increments between 200 to 500 m depth until Day 24 were remarkably similar to the corresponding values from outside water (Fig. 4), indicating little additional flux from the growing bloom. Export from the patch increased steeply after Day 24 but outside loss rates remained constant. Hence, we assume that the background flux from the patch also remained constant until the end of the experiment but was over-ridden by the iron-induced flux event starting between Days 24 and 28. We estimate the total background export from the patch by extrapolating the flux between Days 0 and 24 to Day 36 and subtract this amount from total export to obtain the iron-induced export (Supplementary Methods).

Element losses

A conservative estimate for export of biogenic elements from the 100 m surface layer in the hotspot is the difference between the decline in dissolved inventories (nutrient uptake) and concomitant accumulation in particulate stocks (Supplementary Table 1). Uptake was calculated from the linear regressions depicted in Fig. 3 a - f. Accumulation was estimated as the difference between final and initial stocks of BSi, POP, PON, POC. Initial stocks of particulate elements were taken from the

intercept on Day 0 of the linear regressions until Day 24, and final stocks were the values measured on Day 36 (Fig. 3 g – j). The decline in the DIC inventory of 1.1 mol m^{-2} under-estimates the actual uptake by phytoplankton because of atmospheric CO_2 replenishment. Correcting for air-sea gas exchange adds 0.4 mol m^{-2} to the uptake and hence also to export. The background flux was obtained by extrapolating the losses estimated until Day 24 (0.3 mol C m^{-2}) to Day 36. Iron-induced export of 0.9 mol C m^{-2} (79 mmol C m^{-2} d^{-1} for the 12-day flux event) is obtained by subtracting background flux from total flux estimates (1.4 mol C m^{-2}) for the 36 days of the experiment (Supplementary Table 1).

Correcting budgets based on measured values presented above for mixed layer deepening and diapycnal mixing using the diffusion coefficient of 3.3 10^{-4} m^2 s^{-1} estimated for the EIFEX eddy core[14], about doubles background export estimates inside the hot-spot (from 0.5 to 0.9 mol C m^{-2} or 12 mmol to 26 mmol C m^{-2} d^{-1}) and outside the fertilized patch (from 0.7 to 1.2 mol C m^{-2} or 21 to 36 mmol C m^{-2} d^{-1}). Because nutrient input to the surface layer from below was relatively constant during the 36-day experiment, the correction for iron-induced export during the last 12 days was comparatively minor: from 0.9 to 1.1 mol C m^{-2} or from 79 to 98 mmol C m^{-2} d^{-1}, respectively. Further, correcting the hot-spot budgets for the effects of horizontal dilution (patch spreading) increases total DIC uptake to 2.4 mol C m^{-2} of which 0.6 mol C m^{-2} is exported laterally (Table 1). However, the increase of iron-induced export to 1.2 mol m^{-2} is again minor (Table 1). Dividing the total DIC uptake (2.4 mol C m^{-2}) by the total amount of iron added to the patch water column (0.18 mmol Fe m^{-2}) yields a C/Fe ratio of 13,000 ± 1000 (s.e.m.). This ratio is conservative for reasons discussed in Supplementary Information.

Nitrate (nitrate + nitrite) uptake until the bloom peak on Day 24 (0.17 mol m^{-2}) accounted for 80% of PON production (0.21 mol N m^{-2}), resulting in negative values for background flux not indicated by the other elements (Supplementary Table 2). The decline in DON, via uptake by bacteria and excretion as ammonium to phytoplankton, more than fills the N deficit but its origin is enigmatic. The same amount of DON, but much less DIC, nitrate and phosphate, were taken up outside the patch (Fig. 3, Supplementary Table 3), hence DON contribution to export outside and inside the patch is likely to have been similar. The high variability in ammonium stocks (Fig. 3e) is consistent with rapid turnover within this pool. No clear trends were observed in the subsurface ammonium maxima inside and outside the patch (Supplementary Fig. 4) indicating minor additional accumulation of breakdown products from the flux event in the subsurface layer. The higher C/N ratio for iron-induced export (8.5) compared to lower ratios in suspended POC/PON (~ 5) was also observed during the SOFEX experiment[4].

The steep increase in phosphate stocks on Days 35 and 36 (Fig. 3 c) is only partly explained by leaching from autolysed cytoplasm, due to the well-established greater mobility of this element than carbon[17]. Hence the negative value for exported P due to fertilization (Table 1) is difficult to explain, because unlike the case of N, the source of the additional phosphate during the last 2 days is unknown. Approximately 65% of the silicate taken up was exported during the 37 days of which half can be attributed to iron-induced export at C/Si ratios of 3 and the other half to background flux at a C/Si ratio of 0.8. Outside the patch silicate uptake was slightly lower than inside but all of it was exported in the same period at a C/Si ratio of 0.9 which we attribute to the activity of diatom species that selectively sink silica.

POC export rates from the hotspot estimated from ^{234}Thorium increased steeply from background values <40 mmol C m^{-2} d^{-1} to 125 mmol C m^{-2} d^{-1} during Days 28 – 32 but declined thereafter presumably due to uncertainties associated with short-term sampling by this method (Supplementary Information). Nevertheless, the 2 peak values during the flux event are the highest ever recorded in the Southern Ocean.

Transmissometer profiles

Beam attenuation of the profiling transmissometer was highly correlated with discrete POC measurements across the entire range of concentrations encountered (r^2 = 0.934; $p < 0.001$, Supplementary Fig. 5). Because of the high-resolution vertical coverage of the water column, the depth-integrated transmissometer profiles provide a record of POC accumulation and depletion over depth and time from which export can be estimated[18]. Integrated POC stocks in the upper 3,000 m water column of the patch increased over 37 days by 1.3 ± 0.2 (s.d.) mol C m^{-2} (Fig. 5) implying an accumulation rate of 38 mmol C m^{-2} d^{-1}. The flux event after Day 24 is signalled by steeply increasing POC stocks in the water column below 200 m (Fig. 4) which reached 0.8 ± 0.1 (s.d.) mol C m^{-2} above background levels on Day 36 of which 0.7 ± 0.1 (s.d.) mol C m^{-2} was below 500 m depth (Fig. 5). The increase in deep POC stocks is reasonably close to the corrected estimate of iron-induced export from the surface layer budget (1.2 ± 0.4 (s.d.) mol C m^{-2}), given that some POC had already reached the deep-sea floor as indicated by fresh diatom cells and labile pigments found close to the bottom (Supplementary Fig. 7). Hence losses of iron-induced sinking flux due to underway respiration were apparently minor. Profiles of biogenic barite[16] indicate that only ~ 11% of POC exported during the flux event was remineralised between 200 m and 1000 m. In contrast, the background export until Day 24 was largely respired above 500 m depth as the POC increase below 200 m (Fig. 4) amounted to 0.04 mol C m^{-2} which is <10 % of concomitant loss from the surface layer calculated from corrected element budgets. Identical rates of POC increase in subsurface

layers outside the patch also indicate that background export was remineralised above 500 m depth. We attribute the comparatively high POC stocks in outside waters (0.5 ± 0.1 (s.d.) mol C m^{-2} above background) between 200 and 1000 m on Day 5 and between 300 and 3000 m on Days 33 to 34 (Fig. 4) to slower sinking particle flux from the patchy natural blooms mentioned above (Supplementary Information). Local patchiness in out-stations is indicated by greater scatter in values from successive casts than in in-stations (Fig. 4 & 5).

The steep increase in POC stocks below 200 m under the patch after Day 28 (Fig. 4) can be attributed to POC in the mucilaginous matrix of diatom aggregates in the >1 mm size range which appeared as spikes in the transmissometer profiles. The occurrence of large aggregates reflected in spikiness of the profiles was significantly higher under the hotspot than outside it (Supplementary Fig. 6). Sinking rates of >500 m d^{-1} and aggregates in the centimetre-size range are required to account for the similar slopes of increasing POC at all depths down to the sea floor after Day 28, just 4 days after the enhanced appearance of spikes (aggregate formation) at the pycnocline (Supplementary Fig. 6 a) and visual observation of mass mortality in a major, spiny diatom species, *Chaetoceros dichaeta*. In contrast, the smaller aggregates from the less dense natural blooms sank more slowly than those from the patch. Coagulation models[19,20] of aggregate formation confirm the relationship between sinking rate and bloom density and cell size (including spine length). The latter depends on the species composition of the bloom which thus plays a decisive role in the long-term fate of its biomass.

Organism stocks and rates

Biomass estimates from organism counts were highly correlated with the respective bulk measurements: POC/phytoplankton carbon (PPC) (1.4 mol/mol, $r^2 = 0.54$, $p<0.0001$), PPC/Chl (27 mg/mg, $r^2 = 0.87$, $p<0.0001$) and BSi/total diatom carbon (0.9 mol/mol, $r^2 = 0.76$, $p<0.0001$) which indicated: a) a minor role of particulate organic detritus, b) high cellular chlorophyll content of POC increment by newly accumulated biomass (POC/Chl mg/mg ratio of 32, $r^2 = 0.394$, $p<0.0001$) and c) domination of new biomass by diatoms. Rates of primary production doubled following fertilization and stabilized from Days 9 to 35 at 0.13 mol (1.5 ± 0.1 g) C m^{-2} d^{-1} but declined to 0.08 mol C m^{-2} d^{-1} on Day 36. The total C accumulation and export rates estimated from element budgets are easily accommodated in the 4.2 mol C m^{-2} (51 g C m^{-2}) produced during the bloom. The remainder could be attributed to recycling in the surface layer by bacteria, microzooplankton and copepods whereby grazing pressure on the diatoms was lower than on other protists. Bacterial stocks and production rates declined by ~30 % in the demise phase of the bloom which supports the high transfer efficiency of POC to depth. Thus, the budgets of biological rates are remarkably consistent with other budgets.

In outside water primary production amounted to 1.36 mol C m^{-2} (16 g C m^{-2}) over 34 days which is rather low to accommodate the estimated sinking losses of 1.2 mol C m^{-2} (14.4 g C m^{-2}, Supplementary Table 3) because bacterial remineralisation rates and copepod grazing pressure were in the same range as inside the patch. The discrepancy between measured production and estimated loss rates is partly due to three out stations placed in the sites of previous natural blooms with comparatively low surface DIC inventories (Fig 3 a) but where much of the corresponding POC stocks had already sunk to subsurface layers. Further, the vertical diffusion coefficient applied[14] apparently leads to an overestimation of export. Applying another, twofold higher diffusion coefficient for diapycnal mixing derived from microstructure profiles during EIFEX[15] results in twofold higher export values which are even less supported by direct observations of the plankton community and by POC profiles.

Conclusions

The peak chlorophyll stock of 286 mg m^{-2} is the highest recorded in an OIF experiment to date[5] and demonstrates that, contrary to the current view[21], a massive bloom can develop in a mixed layer as deep as 100 m. The EIFEX results provide support for the second condition of the iron hypothesis[4], that mass sinking of aggregated cells and chains in the demise phase of diatom blooms also occurs in the open Southern Ocean, both in natural[22,23] and artificially fertilized blooms. Given the large sizes, high sinking rates and low respiratory losses of aggregates from the iron-induced bloom, much of the biomass is likely to have been deposited on the sea floor as a fluff layer[24] with carbon sequestration times of many centuries and longer. Larger-scale, longer-term OIF experiments will be required to reduce the effects of horizontal dilution and to further explore the potential of this technique for hypothesis testing in the fields of ecology, biogeochemistry and climate.

METHODS SUMMARY

The eddy was selected on the basis of satellite altimeter and surface chlorophyll distributions. Fertilization was carried out by releasing 7 tonnes of commercial ferrous sulphate dissolved in 54 m^3 of acidified (HCl) seawater into the ship's propeller wash while spiralling out from a drifting buoy at 0.9 km intervals. By day 14 the initial 167 km^2 patch had spread and an area of 740 km^2 was again fertilized with 7 tonnes of $FeSO_4$, this time along east-west transects 3 km apart travelling downstream from north to south (Fig. 1 c).

The patch was located with the drifting buoy and with the photosynthetic efficiency index (F_v/F_m) measured online with a Fast Repetition Rate Fluorometer which, as in previous experiments, was significantly higher in iron-fertilized water. Within a week the bloom had accumulated sufficient

biomass so that additional tracers (chlorophyll and online fCO_2 concentrations) were used to locate the part of the patch least affected by dilution with outside water, i.e. with the highest chlorophyll and, in the last week, the lowest fCO_2 concentrations (Fig 1 c-f). All in-stations were placed inside this "hotspot" and care was taken to locate it with small-scale surveys prior to sampling and to keep the ship within it during the stations which generally lasted about 8 hours. Some in-stations and casts, although within the patch but subsequently shown to have missed the hotspot, have been excluded. For logistical reasons, the out-stations were taken in different locations of the core relative to the patch, i.e. "ahead", "behind" or diagonally opposite it.

Standard oceanographic methods and instruments[15] were used to collect samples and measure the water column properties presented here. See Supplementary Information for details.

References

1. Sigman, D. M. Hain, M. P. & Haug, G. H. The polar ocean and glacial cycles in atmospheric CO_2 concentration. *Nature* **466**, 47-55 (2010).

2. Anderson, R.F. *et al.* Wind-driven upwelling in the Southern Ocean and the deglacial rise in atmospheric CO_2. *Science* **323**, 1443-1448 (2009).

3. Martin, J. H. Glacial-interglacial CO_2 changes: the iron hypothesis. *Paleoceanography* **5**, 1-13 (1990).

4. Coale, K. H. *et al.* Southern Ocean iron enrichment experiment: Carbon cycling in high- and low-Si waters. *Science* **304**, 408-414 (2004).

5. Boyd, P. *et al.* Mesoscale iron-enrichment experiments 1993-2005: synthesis and future directions. *Science* **315**, 612-617 (2007).

6. Cassar, N. *et al.* The Southern Ocean biological response to aeolian iron deposition. *Science* **317**, 1067-1070 (2007).

7. Hamme, R.C. *et al.* Volcanic ash fuels anomalous plankton bloom in subarctic northeast Pacific. *Geophys. Res. Lett.* **37**, L19604 (2010).

8. Lampitt, R. S. *et al.* Material supply to the abyssal seafloor in the Northeast Atlantic. *Prog. Oceanogr*. **50**, 27–63 (2001).

9. Abelmann, A., Gersonde, R., Cortese, G., Kuhn, G. & Smetacek, V. Extensive phytoplankton blooms in the Atlantic sector of the glacial Southern Ocean. *Paleoceanography* **21**, PA1013 (2006).

10. Kohfeld, K.E., Le Quéré, C., Harrison, S. P. & Anderson, R. F. Role of marine biology in glacial-interglacial CO_2 cycles. *Science* **308**, 74-78 (2005).

11. UK Royal Society. Geoengineering the climate: science, governance and uncertainty. The Royal Society Policy Document. London: The Royal Society, London 84 pp. (2009)

12. Chelton, D. B., Schlax, M. G., Samelson, R. M. & de Szoeke, R. A. Global observations of large oceanic eddies, *Geophys. Res. Lett.* **34**, L15606, (2007).

13. d'Ovidio, F., Isern-Fontanet, J., Lopez, C., Hernandez-Garcia, E. & Garcia-Ladona, E. Comparison between Eulerian diagnostics and finite-size Lyapunov exponents computed from altimetry in the Algerian basin. *Deep-Sea Res. I* **56**, 15-31 (2009)

14. Hibbert, A., Leach, H., Strass, V. & Cisewski, B. Mixing in cyclonic eddies in the Antarctic Circumpolar Current. *J. Mar. Res.* **67**, 1-23 (2009)

15. Cisewski, B., Strass, V. H., Losch, M. & Prandke, H. Mixed layer analysis of a mesoscale eddy in the Antarctic Polar Front Zone. *J. Geophys. Res.* **113**, C05017 (2008).

16. Jacquet, S. H. M., Savoye, N., Dehairs, F., Strass, V. H. & D. Cardinal, D. Mesopelagic carbon remineralization during the European Iron Fertilization Experiment. *Glob. Biogeochem. Cycles.* **22**, GB1023 (2008).

17. Paytan, A. & McLaughlin, K. The oceanic phosphorus cycle. *Chem. Rev.* **107**, 563-576, (2007).

18. Bishop, J. K. B., Wood, T. J., Davis, R. E. & Sherman, J. T. Robotic observations of enhanced carbon biomass and export at 55 degrees S during SOFeX. *Science* **304**, 417-420 (2004).

19. Jackson, G.A. A model of the formation of marine algal flocs by physical coagulation processes. *Deep-Sea Res.* **37**, 1197-1211 (1990).

20. Riebesell, U. & Wolf-Gladrow, D. A. The relationship between physical aggregation of phytoplankton and particle flux: a numerical model. *Deep-Sea Res. A* **39**, 1085-1102 (1992).

21. de Baar, H. J. W. *et al.* Synthesis of iron fertilization experiments: From the iron age in the age of enlightenment. *J. Geophys. Res.* **110**, C09S16. doi:10.1029/2004JC002601. (2005).

22. Blain, S., *et al.* Effect of natural iron fertilization on carbon sequestration in the Southern Ocean. *Nature* **446**, 1070-1075 (2007).

23. Pollard, R., *et al.* Southern Ocean deep-water carbon export enhanced by natural iron fertilization. *Nature* **457**, 577-580 (2009).

24. Beaulieu, S. E. Accumulation and fate of phytodetritus on the sea floor. In *Oceanography and Marine Biology. An Annual Review* (eds Gibson, R. N., Barnes, M. & Atkinson, R. J.) 171-232 (Taylor & Francis, London, 2002).

Supplementary Information is linked to the online version of the paper at www.nature.com/nature.

Acknowledgements We thank Christelle Balt, Klaus Loquay, Shine Mkatshwa, Hartmut Prandke, Harald Rohr, Martin Thomas and Ingrid Vöge for help on board. We are also grateful to Ulrich Struck for POC and PON analyses. We thank the captain and crew of RV *Polarstern* for support throughout the cruise.

Author contributions

V.S. and C.K. wrote the manuscript; V.S. directed the experiment, C.K. carried out the budget calculations, V.H.S., P.A., M.M. and D.W.G. contributed to manuscript preparation. V.H.S., B.C., H.L. and M.L. contributed the physical data on mixed layer depth dynamics, eddy coherence, patch movement and transmissometer data. N.S. provided Thorium data. A.W. provided the nutrient data. P.A. and J.H. provided the phytoplankton data. F.D. carried out the Lagrangian analysis based on delayed-time altimetry. J.M.A. and G.J.H. provided the bacterial data. C.N., R.B. provided the inorganic C data. G.M.B., C.K. and M.M.M. provided the POC and PON data, P.C. provided iron data. S.G. and A.T. provided DOM data. I.P. and L.H. performed the ^{14}C primary production measurements and provided HPLC data. R.R. provided data on photosynthetic efficiency (Fv/Fm). C.K., M.S. and A.T. provided Chl data, U.B., E.S., O.S. and J.S. provided data on the eddy core from a subsequent cruise and satellite Chl images.

Author information Reprints and permissions information is available at www.nature.com/reprints. The authors declare no competing financial interests. The readers are welcome to comment on the online version of this article at www.nature.com/nature. Correspondence and request for material should be addressed to V.S. (Victor.Smetacek@awi.de) or C.K. (Christine.Klaas@awi.de).

Table 1. Total and iron-induced export from the hotspot of the fertilized patch

Days	Si	P	NO_2+NO_3	Total N	C
Decrease in stocks of dissolved elements					
0-36	1.14 ± 0.03	0.007 ± 0.003	0.160 ± 0.008	0.33 ± 0.08	1.1 ± 0.2
Input due to air-sea gas exchange					
0-36	-	-	-	-	0.4
Dissolved element input from vertical mixing (diapycnal mixing and deepening of the mixing layer)					
0-36	0.22 ± 0.01	0.011 ± 0.0008	0.059 ± 0.004	0.10 ± 0.01	0.6 ± 0.2
Dissolved element input from horizontal mixing (dilution effect)					
0-36	~ 0	0.010 ± 0.001	0.061 ± 0.005	0.08 ± 0.03	0.26 ± 0.06
Total uptake (decrease of dissolved stocks + gas exchange + vertical mixing + horizontal mixing)					
0-36	1.36 ± 0.03	0.028 ± 0.003	0.28 ± 0.01	0.50 ± 0.09	2.4 ± 0.2
Difference between final and initial particulate matter standing stocks					
0-36	0.28 ± 0.02	0.0062 ± 0.0005	0.081 ± 0.009	0.081 ± 0.009	0.11 ± 0.07
Particulate matter loss by horizontal mixing (dilution effect)					
0-36	0.19 ± 0.02	0.0089 ± 0.0004	0.110 ± 0.006	0.110 ± 0.006	0.58 ± 0.04
Vertical export (Total uptake - difference in particulate stocks - particulate loss by horizontal mixing)					
0-36	0.89 ± 0.04	0.013 ± 0.003	0.09 ± 0.02	0.31 ± 0.09	1.7 ± 0.2
Background (vertical) export*					
0-36	0.50 ± 0.07	0.025 ± 0.003	*-0.06 ± 0.03*	0.18 ± 0.06	0.5 ± 0.3
Vertical export due to fertilization (vertical export - background export)					
24-36	0.40 ± 0.08	-0.012 ± 0.005	nd	0.1 ± 0.1	1.2 ± 0.4

Budgets were calculated for the surface layer (0-100 m) from the beginning of the fertilization experiment (Day 0) until the last station carried out inside the fertilized patch (Day 36) (see Supplementary Methods for details). All values are in mol m^{-2}. Uncertainties (s.e.m.) were estimated by propagation of standard errors based on linear uptake models (Fig. 3) and measurement uncertainties. * Vertical export between days 0 to 24 (0.4 mol C m^{-2}, Supplementary table 3) extrapolated to 36 days (Supplementary Methods).

Figure 1 | The experimental eddy and the fertilized patch. a. The eddy core depicted with the streamfunction derived from currents measured with a vessel-mounted acoustic Doppler current profiler at a regular grid of stations completed from Days 1 – 7 and location and cruise track of the initial fertilization on Day 0. The blob is the ship's track (a Lagrangian circle) around the buoy drifting south-westward during fertilization. White oval is the superimposed track of the drifting buoy during its first rotation from Days -1 to 11 (same as in panel b and c). b. Altimeter image of sea-surface height anomaly, scale bar in cm (http://argo.colorado.edu/~realtime/gsfc_global-real-time_ssh/). The rectangle in panel a and b is blown-up in panels c - f. c. Area and location of the patch on Days 10 to 11 after fertilization based on chlorophyll measurements. The yellow area is the "hot-spot". d-f. Location and area of the patch 17 days after fertilization depicted with Fv/Fm ratios (d), *f*CO2 concentrations (e) and chlorophyll concentrations (f). The line is the track of the drifting buoy during its second rotation from Days 13 – 21. The red area in f is the hot-spot. g-i. Satellite-derived surface chlorophyll concentrations of the EIFEX eddy before fertilization (g), during the bloom peak (h) and in its demise phase (i). The eddy core is encircled in white in the panels, the EIFEX bloom is evident in the second (h) and third panels (i). Note the natural bloom along the Polar Front which disappeared in this period. SeaWifs images courtesy of the NASA SeaWiFS Project and GeoEye.

Figure 2 | Temporal evolution of chlorophyll and silicate concentrations. Chlorophyll concentrations reflect the growth, peak and demise phases of the bloom in the patch (a) in contrast to the low values outside it (b). The slightly higher out-patch values in the beginning are due to local patchiness in outside water and not interim accumulation. The declining trend of silicate in outside water (d) is interrupted by local patchiness in contrast to the smooth trend in the patch (c). Note variations in mixed layer depth below 100 m. Black diamonds indicate depth of discrete samples.

Figure 3 | Time course of dissolved and particulate elements. Values inside (filled circles) and outside (open circles) the fertilized patch are depth-integrated average concentrations for the upper 100 m of the water column. Lines represent the temporal evolution inside the patch (full line) and outside the fertilized patch (broken line) used in elemental budget calculations (Supplementary Methods) determined by linear regression. The r^2 for the models are 0.64 (DIC), 0.88 (nitrate+nitrite), 0.74 (phosphate), 0.97 (silicic acid), 0.33 (ammonium), 0.63 (DON), 0.84 (POC), 0.94 (PON), 0.93 (POP), 0.96 (BSi), 0.92 (Chl), 0.05 (DOC) inside the patch and 0.06 (DIC), 0.24 (nitrate + nitrite), 0.13 (phosphate), 0.71 (silicic acid), 0.24 (ammonium), 0.58 (DON), 0.84 (POC), 0.64 (PON), 0.85 (POP), 0.008 (BSi) and 0.005 (DOC) outside the patch. All regressions are

significant with $p < 0.005$ with the exception of in-patch DOC ($p = 0.4$) and out-patch DIC ($p = 0.5$), nitrate + nitrite ($p = 0.011$), phosphate ($p = 0.1$), ammonium ($p = 0.02$), DON ($p = 0.046$), PON ($p = 0.03$), BSi ($p = 0.8$) and DOC ($p = 0.8$).

Figure 4 | Time course of particulate organic carbon stocks in successive depth layers. Stocks for the respective layers are derived from depth-integrated, vertical profiles of beam attenuation of a transmissometer calibrated with discrete POC measurements (black symbols). Left and right panels are for inside and outside the patch, respectively. Note different scales of the Y axes. Depth intervals of integrations are (a, i) 0–100 m depth, (b, j) 100–200 m depth, (c, k) 200–300 m depth, (d, l) 300–400 m depth, (e, m) 400–500 m depth, (f, n) 500–1000 m depth, (g, o) 1000–2000 m depth and (h, p) 2000–3000 m depth. Lines are derived from linear regression models. Variability in stocks and trends in the 100-200 m depth layers is due to intermittent shoaling and deepening of the particle-rich, surface mixed layer between 100-120 m, possibly due to the passage of internal waves. The high values on Days 5 and 34 out-patch are not included in the regressions. The layer below 3,000 m is not included to avoid contamination by resuspended sediments in the nepheloid layer. Red diamonds are integrated stocks from measurements on discrete water samples. Variability in these values is due to low depth resolution, particularly below 500 m depth.

Figure 5 | Depth-integrated particulate organic carbon stocks. Stocks for the water columns 0 – 500 m (triangles) and 0 – 3,000 m (circles) are derived from vertical transmissometer profiles as in Fig. 4. Left and right panels are for inside and outside the patch, respectively. All profiles taken to the sea floor during the study are depicted. Because the depth of the flux event was not anticipated and deep casts are time consuming, only 6 profiles to the sea floor were taken prior to the flux event: one pre-fertilization, one in the hotspot, two outside the patch of which one was inside the core and 2 in the APF meander.

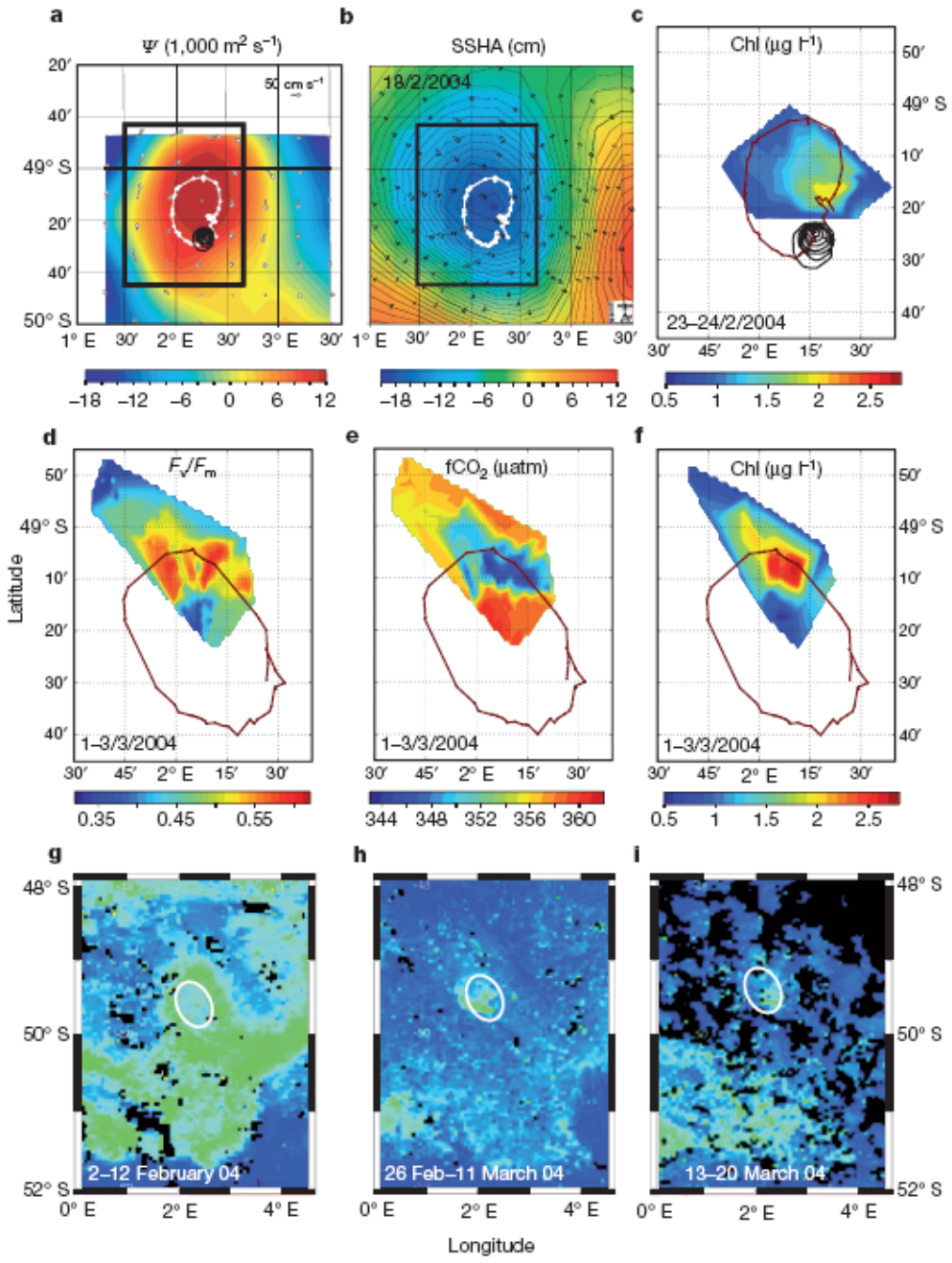
a
Ψ (1,000 m² s⁻¹)
50 cm s⁻¹
b
SSHA (cm)
18/2/2004
c
Chl (μg l⁻¹)
23–24/2/2004
d
Fv/Fm
1–3/3/2004
e
fCO2 (μatm)
1–3/3/2004
f
Chl (μg l⁻¹)
1–3/3/2004
g
2–12 February 04
h
26 Feb–11 March 04
i
13–20 March 04
Latitude
Longitude

Figure 1

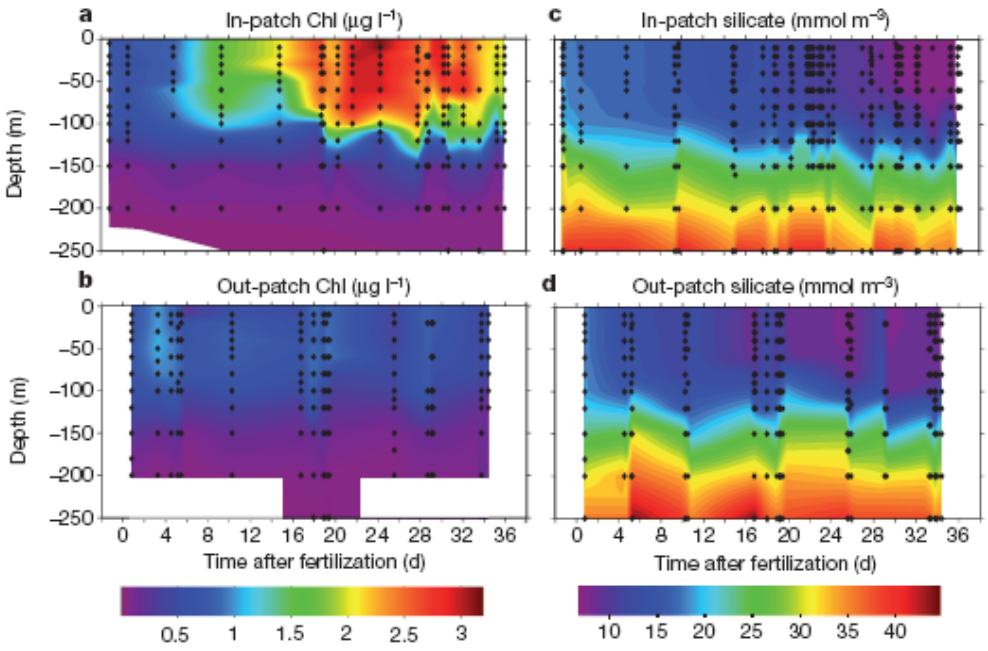
a
In-patch Chl (µg l−1)
c
In-patch silicate (mmol m−3)
b
Out-patch Chl (µg l−1)
d
Out-patch silicate (mmol m−3)
Depth (m)
0
−50
−100
−150
−200
−250
0 4 8 12 16 20 24 28 32 36
Time after fertilization (d)
0.5 1 1.5 2 2.5 3
10 15 20 25 30 35 40

Figure 2

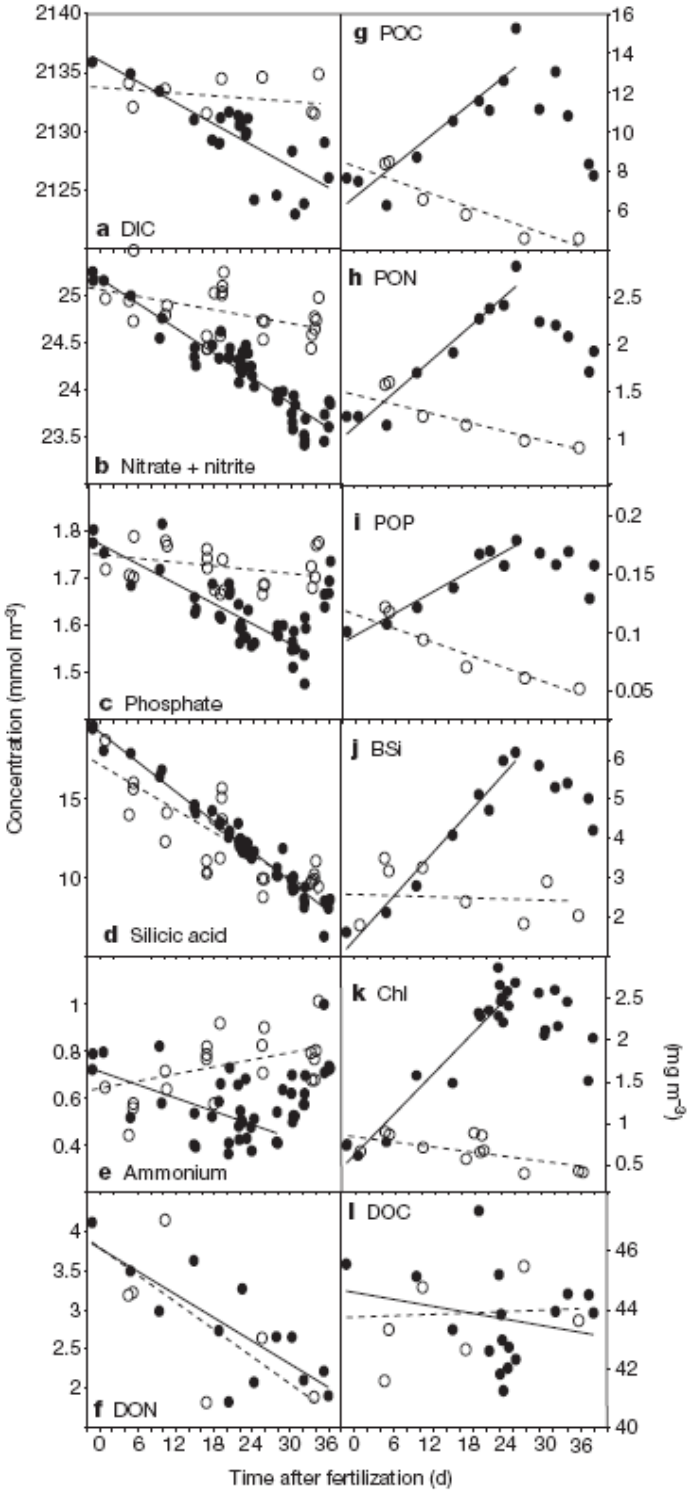
a DIC
b Nitrate + nitrite
c Phosphate
d Silicic acid
e Ammonium
f DON
g POC
h PON
i POP
j BSi
k Chl
l DOC
Concentration (mmol m⁻³)
(mg m⁻³)
Time after fertilization (d)
0 6 12 18 24 30 36

Figure 3

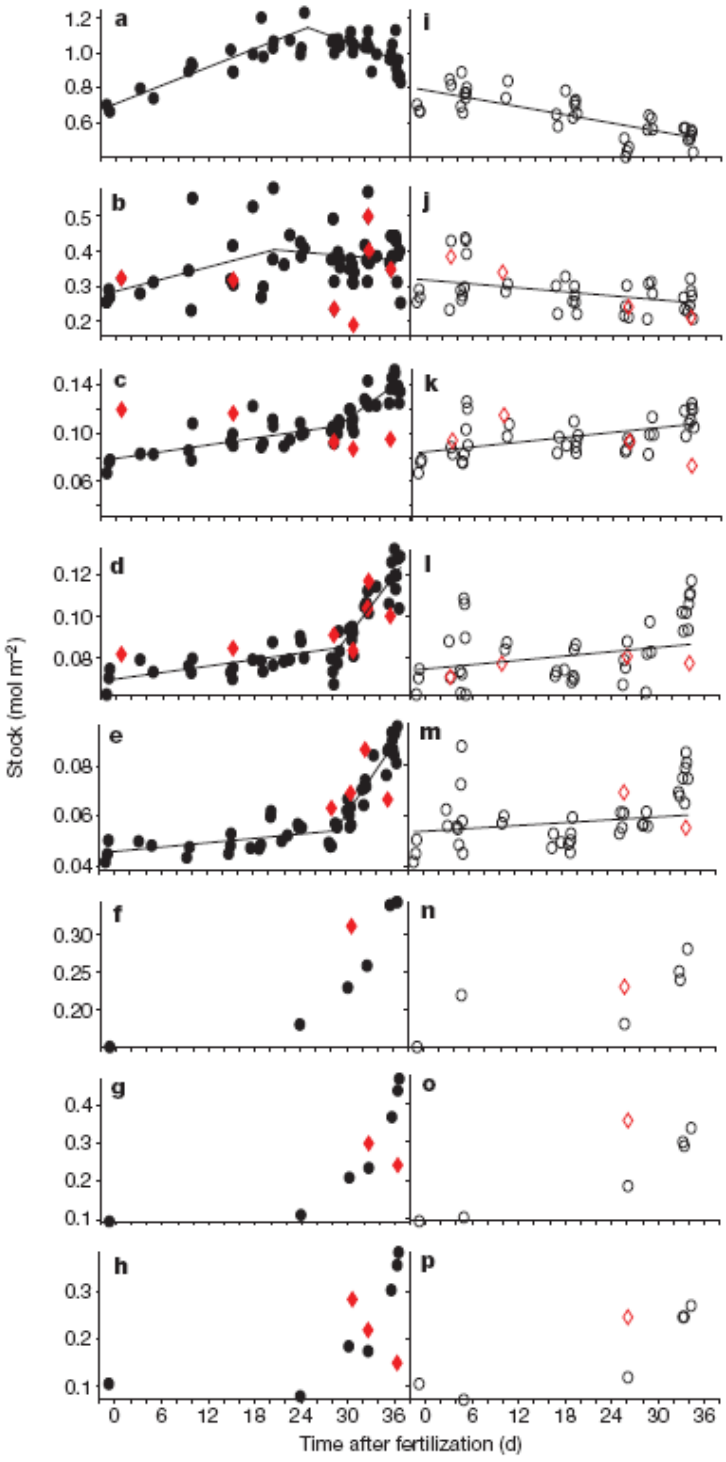

Figure 4

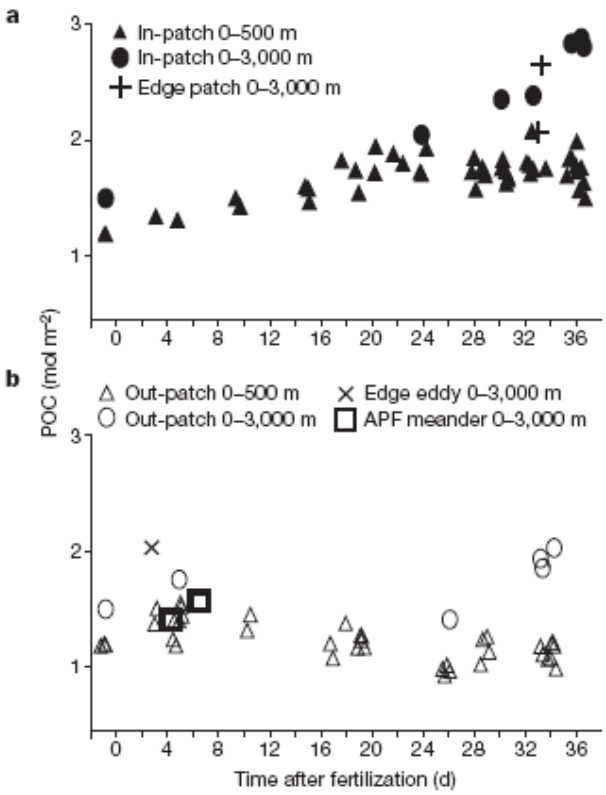
a
In-patch 0–500 m
In-patch 0–3,000 m
Edge patch 0–3,000 m
b
Out-patch 0–500 m
Out-patch 0–3,000 m
Edge eddy 0–3,000 m
APF meander 0–3,000 m
POC (mol m⁻²)
Time after fertilization (d)

Figure 5